Available online at www.sciencedirect.com
ScienceDirect
Journal of Asian Earth Sciences 31 (2007) 251–264
Journal of Asian Earth Sciences
www.elsevier.com/locate/jaes

Active deformation front delineated by drainage pattern analysis and vertical movement rates, southwestern Coastal Plain of Taiwan

Chih-Cheng Barry Yang [a,*], Wen-Shan Chen [a], Leh-Chyun Wu [b], Chii-Wen Lin [c]

[a] Department of Geosciences, National Taiwan University, Taipei 106, Taiwan
[b] Department of Geology, Chinese Culture University, Taipei, Taiwan
[c] Central Geological Survey, MOEA, Taipei, Taiwan

Received 25 February 2004; received in revised form 18 September 2005; accepted 27 July 2006

Abstract

Orogenesis in Taiwan results from an arc-continent collision between the Eurasian plate and the Philippine Sea plate. The southwestern part of Taiwan absorbs active shortening as evidenced by rapid crustal deformation and frequent earthquakes. Southwestern Taiwan may be subdivided into three tectonic–geomorphic domains, including the plain (PL), the tilted tableland (TT), and the low hills (LH), based on geomorphology, drainage pattern and stratigraphic records. The PL domain is the westernmost and is characterized by meandering rivers with relatively low surface slope and river gradient, but high river sinuosity. The TT domain has slightly tilted terraces with river meanders and many tributaries are developed on its surface. Anomalous river sinuosity occurs as a result of active tectonics. The LH domain has higher elevation and deformed geomorphic surfaces associated with a dissected landscape. This domain also has high stream gradients with low sinuosity which may indicate active deformation. We define crustal deformation, using Holocene deposits and radiocarbon dating in addition to geomorphic analysis that suggests a blind thrust may exist between the PL and TT domains. This blind thrust may indicate the position of the active deformation front of the orogenic belt of southwest Taiwan.

Keywords: Deformation front; Blind thrust; Drainage pattern; Digital Elevation Model (DEM)

1. Introduction

Taiwan is located in the junction between the Eurasian plate and the Philippine Sea plates. This oblique arc-continent collision is propagating from north to south (Suppe, 1981, 1984; Teng, 1990; Teng et al., 2000), and this governs the development of Taiwan orogen and defines four geological terranes. From west to east, these terranes, respectively, include the Coastal Plain, Foothills Belt, Backbone Range and the Coastal Range. Rapid uplift and frequent earthquakes in Taiwan indicate that this plate collision is ongoing. The location of the deformation front of the Taiwanese orogen remains a key question for hazard assessment. Ho (1967) considered that the westernmost border of the Foothills is the deformation front of the fold-and-thrust belt. In contrast, Biq (1992) proposed that a major thrust fault may be situated along the westernmost part of Coastal Plain as a result of basement collision. Liu et al. (1998) argued that the deformation front might be easily recognized as the northern extension of the Manila Trench based on submarine topographic depression (Fig. 1a). However, it is unclear where the location of deformation front is on land in southern Taiwan due to extremely high rates of sedimentation from the mountain belt to the east. Recently, Deffontaines et al. (1997) suggested that the deformation front may be situated along the western margin of the Tainan tableland (TN) and extends northward (Fig. 1b), but this is uncertain because obvious topographic features are unknown in this region. Meanwhile, Sun et al. (1998) showed that, based on a shallow seismic reflection

* Corresponding author. Tel.: +886 2369 2594; fax: +886 2363 6095.
E-mail address: d91224003@ntu.edu.tw (C.-C.B. Yang).

1367-9120/$ - see front matter © 2007 Elsevier Ltd. All rights reserved.
doi:10.1016/j.jseaes.2006.07.026

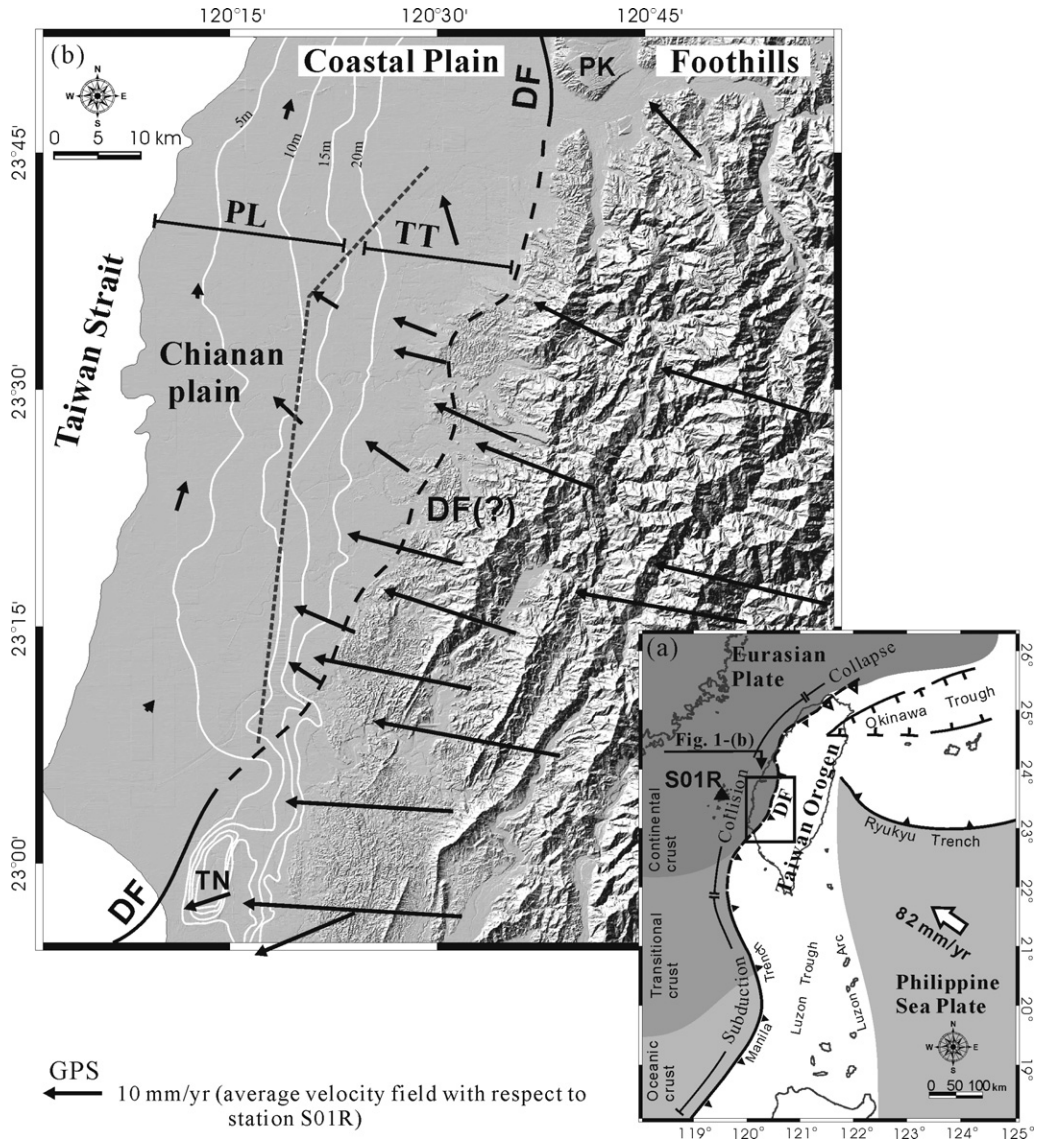

Fig. 1. (a) Tectonic framework around Taiwan. The deformation front is created by the arc-continental collision between the Eurasian plate and the Philippine Sea plates. Arrow indicates the direction of convergence (Modified from Teng et al., 2000). (b) Shaded topographic map of southwestern Taiwan obtained from 40-m Digital Elevation Modal. Deformation front (DF) can be identified along the western borders of the Tainan Tableland (TN) and Pakau (PK) Tablelands (solid line), but it is not clear in the section in between. Previous studies locate it along the hill front (thick-dash line) (Ho, 1967). The thin-gray dashed line in Coastal Plain divides, tentatively, Chianan plain into the plain domain (PL) and tilted tableland domain (TT). South part of the gray dashed line is suggested along the 10 m contour with a flat plain to the west and tilted surface to the east can be related to contraction recorded by GPS data (Yu et al., 1997). The bending of the gray dashed line is inferred from GPS data marking a change in direction from west to northwest movement.

study, deformed Holocene strata beneath exist the Chianan plain in the southern part of Coastal Plain. Geodetic data also show that crustal strain accumulated in the Chianan plain (Fig. 1b) (Yu et al., 1997; Hsu et al., 2003). Frequent historical earthquakes beneath the Coastal Plain also indicate that it is tectonically active (Cheng and Yeh, 1989). Thus, the eastern part of the Chianan plain is probably the westernmost leading edge of the Taiwan orogen. Since the Chianan plain may be considered to be tectonically active and it has a dense population, delineating location of active faults and folds is urgently needed.

We show that the deformation front of the Taiwan orogen may have migrated westward into Coastal Plain and west of the Foothills domain. However, our interpretation is controversial because Holocene deposits cover the entire area of central and southern Coastal Plain. In this paper, we analyze the drainage pattern and stratigraphic records of the Chianan plain. We would make looked for a steepening of river gradients to mark the westernmost point of uplift in the belt. Borehole data are used for calculating the rates of vertical crustal movement. Based on these data we locate a hinge line between uplift and subsidence.

2. Geological setting and geomorphology

The study area on the west side of Taiwan includes the outer part of the Foothills Belt and Coastal Plain, geomorphic domains that correlate with the fold-and-thrust belt and foreland basin of the Taiwanese Orogeny. The outer part of the Foothills domain can be subdivided into lower hills on the west and higher hills on the east, and their boundary is recognized as a mountain front where several NNE-striking, west-vergent thrusts have been mapped (Fig. 2) (Sun, 1970, 1971; Hung et al., 1999; Lin et al., 2000).

The strata exposed in the study area are shown in Figs. 2 and 3. The lithostratigraphic units differ across the Niouchou River. Strata exposed north of the Niouchou River reveal a coarsening upward sequence of coastal to alluvial sediments. These deposits are associated with the leading edge of the fold-and-thrust belt and are linked to rapid evolution of the mountain belt. In the south, the strata show a coarsening upward sequence with much finer sediment. The southern sequence was deposited in an offshore coastal environment. The change in lithology north and south of the Niouchou River is not a consequence of tectonism but a change in depositional setting. Recently, these two depositional sequences have been tied into nearly the same age (Plio-Pleistoence) with nannofossils, paleomagnetic and petrographic analysis as shown in Fig. 3c (Chen et al., 1992, 2000, 2001).

Structures in the southwestern Taiwan can be divided into several regions from north to south based on the structural pattern and geomorphic features (Mouthereau et al., 2002; Shyu et al., 2005). The study area is in the Chiayi neotectonic block, which is bounded by the Kukeng fault to the north, the Hsinhua fault to the south and the Chukou–Lunhou fault to the east (Fig. 2). A series of thrusts exists in the lower hills near the mountain front in the northern part of the study area that include the Hsiaomei and Chiuchiungkeng faults (Fig. 3a; Hung et al., 1999; Yang et al., 2003). The areas bounded by these faults are characterized by different geomorphic features, plain west of the Hsiaomei fault, tablelands in the central area, and a dissected region east of the Chiuchiungkeng fault (N–N′ in Fig. 3a). In the southern part of the study area, two active faults are identified, the Liouchia and Lunhou faults (S–S′ in Fig. 3b). However, west of the Liouchia fault, the ground surface has been gently tilted to the west, suggesting the presence of a blind thrust. The thrust is the southern counterpart of the Hsiaomei blind fault to the north. The geomorphic characteristics of this southern part can also be divided into the three domains, namely plains, tablelands and low hills.

Two large destructive earthquakes occurred in 1906 and 1946 (Chang et al., 1947; Bonilla, 1975; Yeh et al., 1984; Biq, 1991) within the Chiayi block, and are associated with two right-lateral strike-slip surface ruptures on the Meishan and Hsinhua faults (Fig. 2). The location of the western boundary of Chiayi block is still under debate because tectonic structures are buried there by young sediments.

3. Analytical methods

3.1. Drainage pattern recognized from DEM

Landscapes in actively deforming areas result from the interaction of tectonic and surface processes. In young orogens, rapid sedimentation can obscure young structure. In such situations, geomorphic indices are useful to discriminate the type of landscape generating process (Burbank and Anderson, 2001). In particular, the analysis of the drainage pattern can help elucidate the location of active structures.

We tentatively divided the study area into three geomorphic domains; the plain (PL), tilted tableland (TT), and lower hills (LH) domains. Five rivers cross the three domains transversely, and all originate from the eastern boundary of the higher hills, implying that the modern river valleys developed since the formation of the boundary faults (i.e. the Chukou and Lunhou faults as shown in Fig. 2). All five rivers are characterized by meandering channels (Fig. 4). Meanders typically develop under conditions of limited bed-loads, fine-grained sediments and low river-bed gradient (Schumm et al., 2000). These conditions are imposed by catchment size. The catchment areas of rivers in the study area are all less than 300 square kilometers, except the southernmost one. These areas represent one half to one fifth of all other catchments in western Taiwan.

The density of tributaries increases in both the TT and LH domains, exhibiting a dendritic pattern (Fig. 4). Since the modern meanders in the PL domain have no dendritic pattern of tributaries, we infer that they may be recording by crustal deformation caused by active uplift. Based on these observations, we quantitatively analyze river profiles to identify structural features across these domains.

We digitized the topography of river valleys from the 1:25,000 topographic maps, and used a 40-m DEM to measure the river profiles as well as the drainage pattern. Our results include estimates of surface slope, river gradient and river sinuosity in each domain (Figs. 4 and 5). Comparison of river profiles and drainage patterns show very distinct features for each domain. The PL domain displays relatively low surface slope ($s_S = 0.5$ m/km) and river gradient ($g_R = 0.2$ m/km), but a high river sinuosity ($S = 1.4$). In the TT domain the surface slope rapidly increases eastwards compared to the PL, especially in the northern area where an anticline is located (in river A, $s_S = 7.1$ m/km). Stream gradients in the TT domain also increase eastwards, although not as rapidly as surface slope. Sinuosity is anomalously high (in river A, $S = 1.6$; in river D, $S = 1.7$). The anomalously high sinuosity is a consequence of movement on active structures as suggested by stream-table experiments (Schumm and Khan, 1972; Burnett and Schumm, 1983; Ouchi, 1985). The incised-meandering channel with dendritic tributaries is a

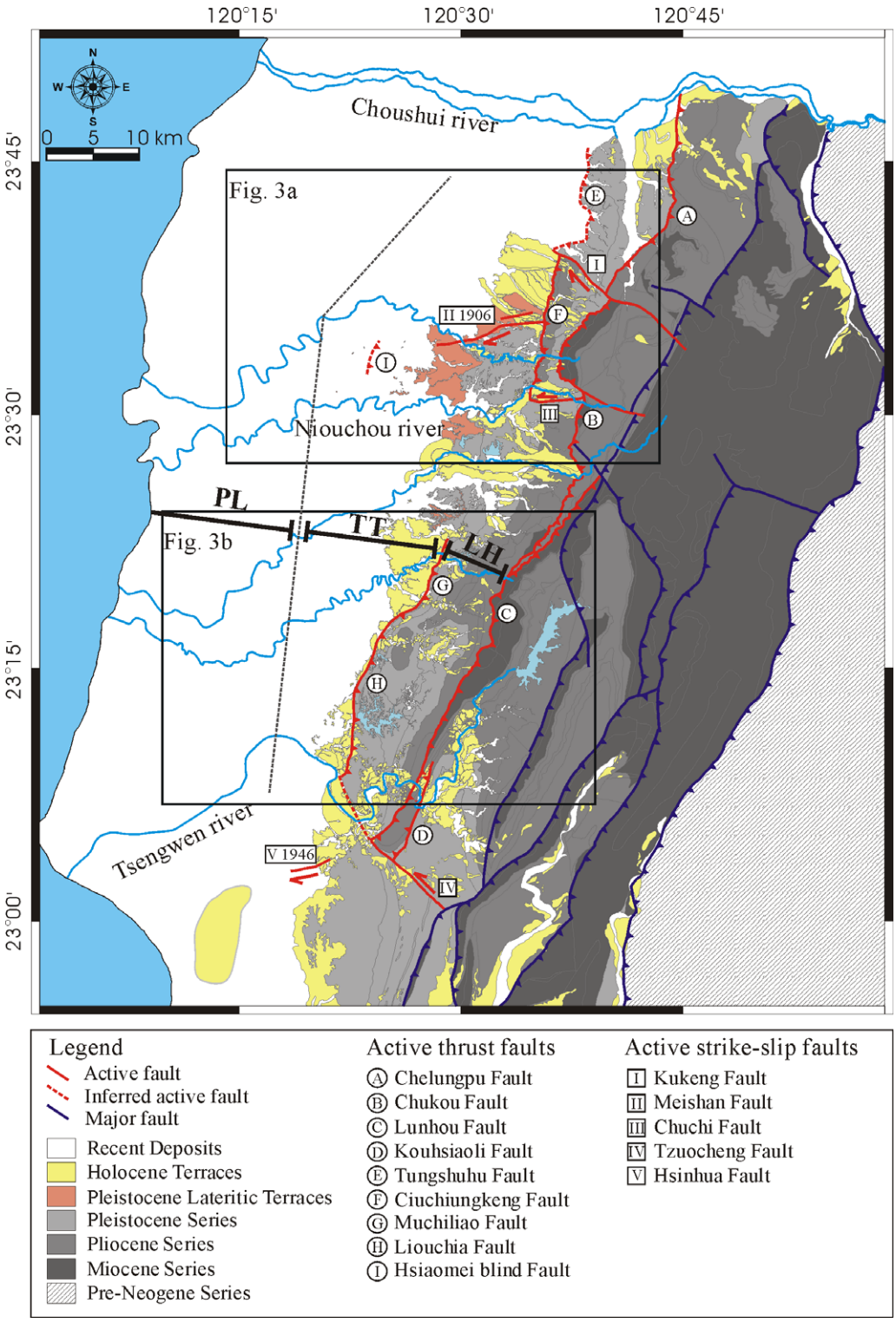

Fig. 2. Geologic map of southwestern Taiwan. Several active faults (red lines) are located along the westernmost side of the Foothills. The study area is, respectively, bounded by the Kukeng and Hsinhua faults to the north and the south (adapted from Chinese Petroleum Corporation, 1986, 1989). The low hills (LH) domain is located between two active boundary faults in the western Foothills: the Chukou–Lunhou faults in the east and the Ciuchiungkeng–Muchiliao–Liouchia faults in the west.

consequence of uplift in the TT domain and younger terraces have formed along the meanders (Fig. 4a and b). In the easternmost area, the LH domain shows deeply dissected landscapes. The increase in stream gradient and the decrease in sinuosity is interpreted to indicate long-term uplift. As discussed above, the boundary faults between the TT and the LH domains are interpreted to be responsible for the differential uplift.

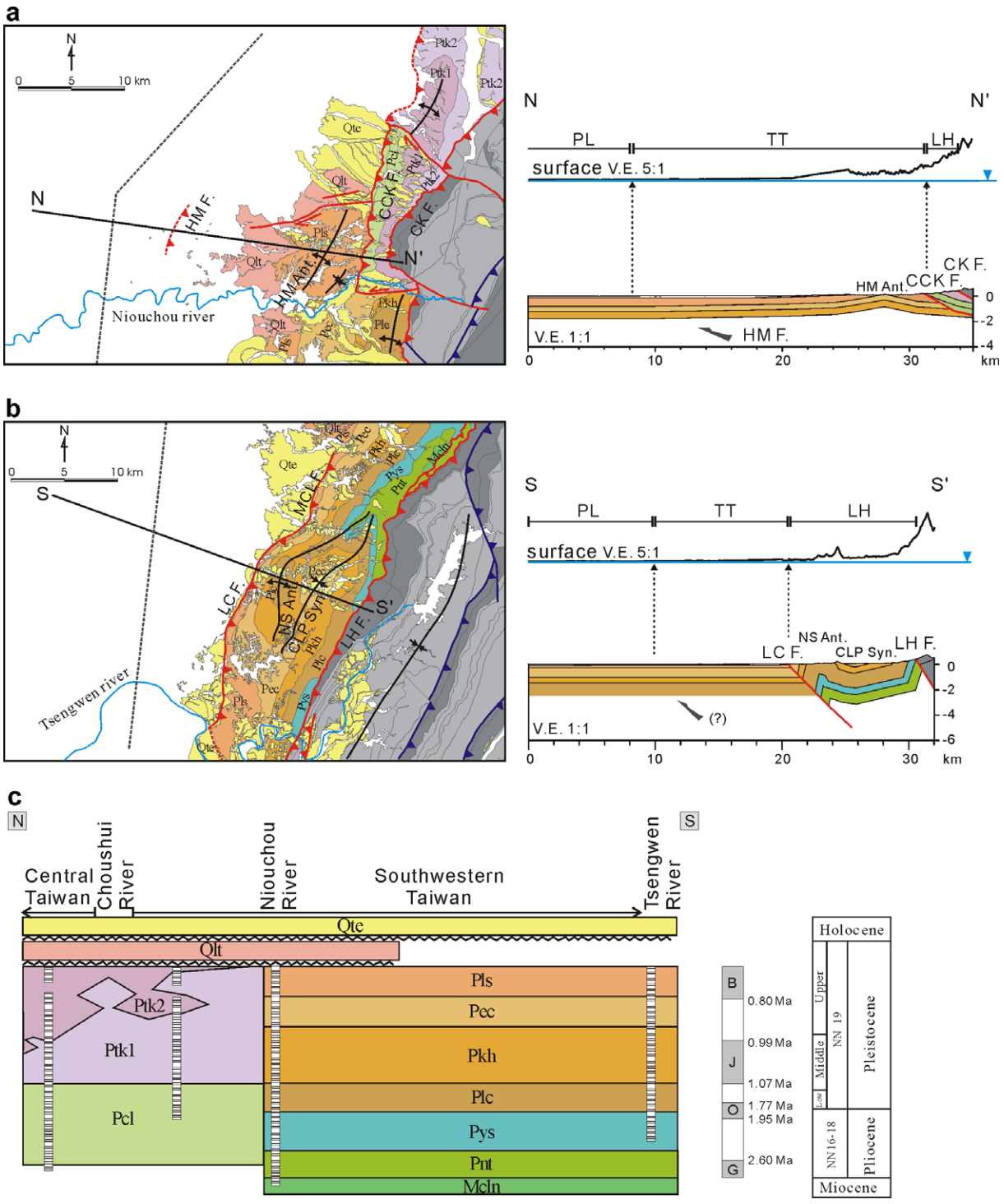

Fig. 3. Regional geologic maps of the northern part (a) and southern part (b) of the study area. The Miocene–Pleistocene strata units lies in the hanging wall of the Chukou and Lunhou faults are shown in the Fig. 2. The Plio-Pleistoence strata units between active faults are shown in (c). In the N–N′ cross section, the low hills (LH) domain lies between the Chukou and Ciuchiungkeng faults. The tilted tableland (TT) domain lies between the Ciuchiungkeng and Hsiaomei blind fault. The plain (PL) domain is situated west of the Hsiaomei blind fault. Note the difference in relief in the TT domain and the location of the subsurface structure in LH and TT domains between cross section S–S′ and N–N′. CK F., Chukou Fault; CCK F., Ciuchiungkeng Fault; HM F., Hsiaomei Fault; LH F., Lunhou Fault; LC F., Liouchia Fault; HM Ant., Hsiaomei anticline; NS Ant., Nioushan anticline; CLP Syn., Chientapu syncline; V.E., Vertical exaggeration. (c) The exposed rock strata in the study area are correlated based on nannofossils, petrography and paleomagnetic study (modified from Chen et al., 2000). Lithostratigraphic units in the northern part of the Niouchou River: Pcl, Cholan Formation; Ptk1, Toukoshan Formation (sandstone dominated); Ptk2, Toukoshan Formation (conglomerate dominated); Qlt, Lateritic deposits; Qte, terrace deposits. Lithostratigraphic units in the southern part of the Niouchou River: Mcln, Chunlun Formation; Pnt, Niaotsui Formation; Pys, Yunshuichi Formation; Plc, Liuchungchi Formation; Pkh, Kanhsialiao Formation; Pec, Erhchungchi Formation; Pls, Liushuang Formation; Qlt, Lateritic deposits; Qte, terrace deposits. G, Gauss; O, Olduvai; J, Jaramillo; B, Brunhes.

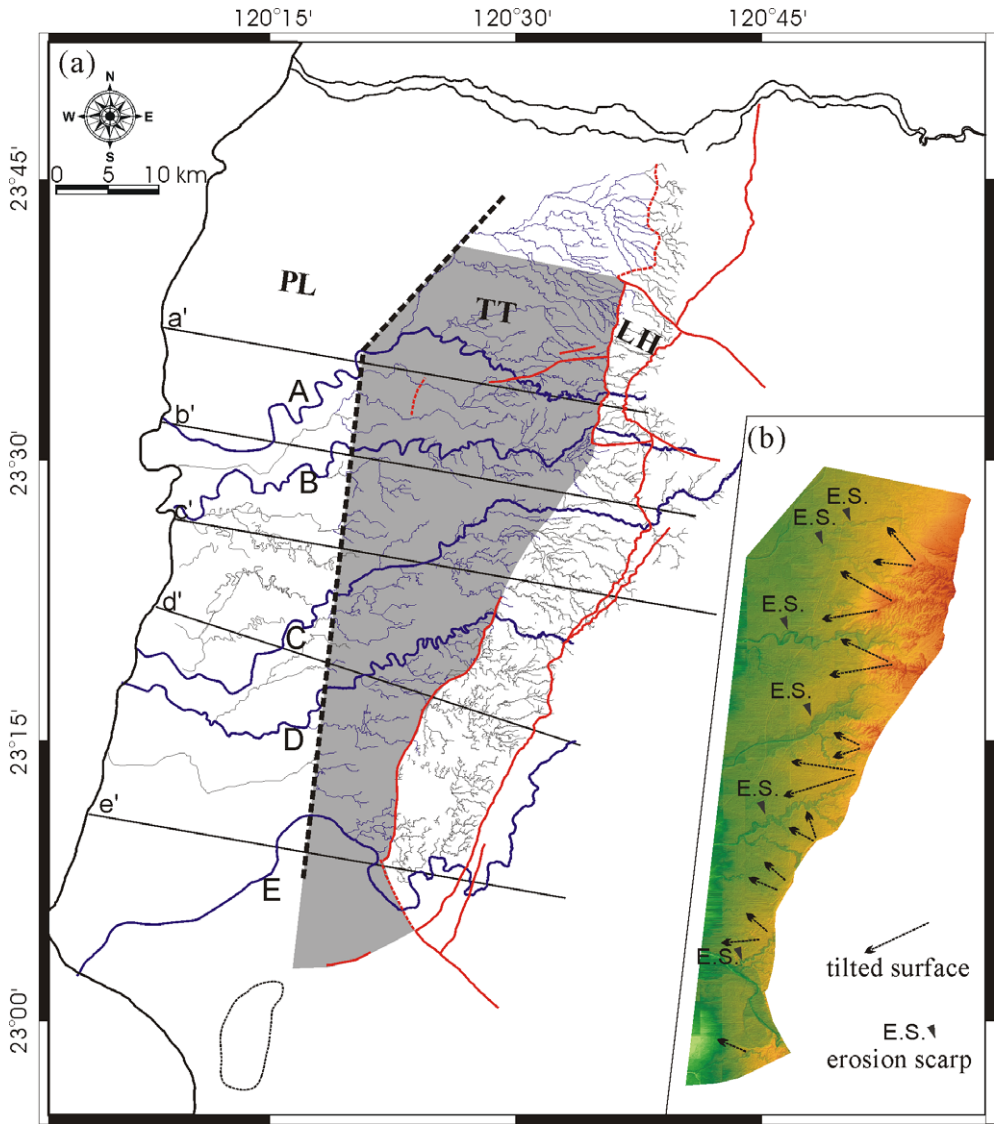

Fig. 4. (a) Drainage pattern of the study area obtained from 1:25,000 scale topographic maps, using 40-m DEM. Five major rivers (A–E, thick-blue line) are projected onto NE–SW profiles (a′–e′; parallel to convergence direction as suggested from GPS and geological data). River profiles are used to analyze the neotectonic influence across all the three domains and are shown in Fig. 5. The red lines are active faults as shown in Fig. 2. (b) The TT domain, is characterized by erosional scarps (E.S.), tilted surfaces (arrows) and the dendritic pattern of tributaries (thin-blue line in Fig. 4a). These characteristics are used to divide the Coastal Plain into two geomorphic domains (i.e. the PL and TT domains). A, Peikang River; B, Niouchou River; C, Pachang River; D, Jishui River; E, Tsengwen River.

3.2. Recent crustal movements derived from borehole data

We next calculate the vertical movement rates from borehole data to further constrain active shortening in the PL and TT domains. Information from 34 cores drilled in late Pleistoence and Holocene sediments in the PL and TT domains are used to calculate recent crustal movements (Table 1, Fig. 6). The depositional depth is assumed as 0–3 m for marsh environment, 0 to −3 m for estuary, lagoon environment, and tidal-channel, −1 to −10 m for shoreface to upper offshore environments (Shirai and Tada, 2000). The relative vertical crustal movement can be derived by comparing the depths of different age horizons. The absolute value is obtained by correcting for eustatic sea-level change (Hanebuth et al., 2000). The formula to compute the rate of vertical crustal movements is:

$$U_t = (E_{\text{sample}} - E_{\text{sea-level}} - D)/T$$

where U_t is the rate of vertical movement (mm/yr); E_{sample}, the elevation of the sample relative to the modern sea level; $E_{\text{sea-level}}$, the elevation of eustatic sea level at the depositional time of the sample; D, the sample's depositional depth or height; and T is the radiocarbon age of the sample. The eustatic sea-level curve is adopted from previous studies in Taiwan (such as Chen and Liu, 1996, 2000).

For the purpose of comparing the movement rate with different cores for similar time periods, the corresponding

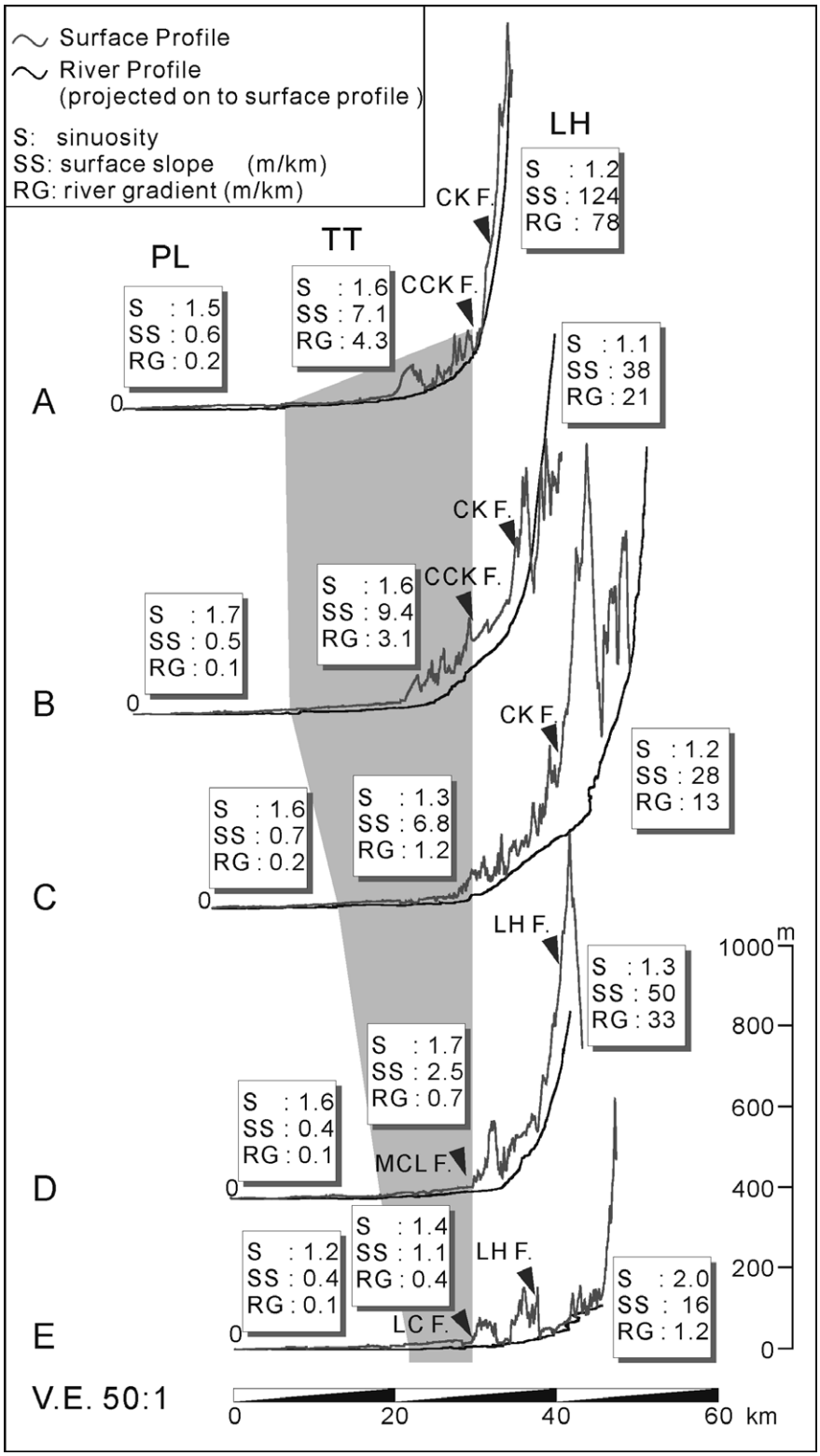

Fig. 5. Surface and river profiles for major rivers (A–E river in Fig. 4) across the three geomorphic domains (PL, TT and LH). Distinct geomorphic factors such as river sinuosity and river gradient can be compared with surface slope in each domain. V.E., vertical exaggeration.

radiocarbon ages of selected samples are all younger than 10,000 yrs. Information on the sedimentary environments is adopted from previous work by Wu (1999).

Although the vertical movement rates depend on the assigned depositional depth, the general uplift–subsidence pattern can be compared across boreholes. Data from four

Table 1
Data from boreholes and calculated vertical movement rates

ID	Location		Sample elevation[a] (m)	C-14 age (yrs BP)	Calibrated age[b] (2σ) (cal. yrs BP)	Paleo-sea level[c] (m)	Depositional depth[d] (m)	Vertical movement rate (mm/yr)		
	lat. (°)	long. (°)						max.	min.	average
A	23.5787	120.3016	−33.1	8440 ± 90	9154–9550	−26 to −23	−3 to 0	−0.4	−1.1	−0.8
B	23.5549	120.3499	−34.1	9440 ± 70	10432–11070	−49 to −38	−3 to 0	1.6	0.4	1.0
C	23.5574	120.4355	−4.2	8460 ± 70	9301–9547	−26 to −24	0–3	2.3	1.8	2.0
D	23.4602	120.1543	−42.2	8700 ± 70	8956–9748	−28 to −22	−10 to −1	−0.4	−2.1	−1.3
E	23.4596	120.2394	−50.6	9930 ± 190	10758–12308	−57 to −44	−3 to 0	0.8	−0.6	0.1
F	23.4852	120.3350	−39.3	9999 ± 60	11630–11931	−55 to −50	−3 to 0	1.6	0.9	1.2
G	23.4390	120.2765	−40.4	10340 ± 160	11344–12876	−61 to −50	−3 to 0	1.8	0.8	1.3
H	23.4114	120.2496	−53.4	9880 ± 40	11196–11337	−50 to −49	−3 to 0	0.0	−0.4	−0.2
I	23.4169	120.3816	−15.8	9517 ± 67	10578–11157	−49 to −40	−3 to 0	3.2	2.3	2.8
J	23.3566	120.2192	−49.7	9650 ± 80	10695–11201	−49 to −43	−3 to 0	0.2	−0.6	−0.2
J-1	23.3566	120.2192	−90.6	37520 ± 1550			Using for correlation in Fig. 7			
J-2	23.3566	120.2192	−138.8	37860 ± 390			Using for correlation in Fig. 7			
K	23.3299	120.2605	−28.3	8180 ± 250	8144–9291	−24 to −15	−10 to −1	0.6	−1.5	−0.4
L	23.3528	120.4132	10.0	7250 ± 100	7865–8320	−17 to −13	−3 to 0	3.6	2.9	3.3
M	23.2962	120.1689	−83.0	9806 ± 57	11161–11296	−50 to −49	−3 to 0	−2.7	−3.0	−2.9
N	23.2608	120.2078	−37.5	8260 ± 160	8724–9542	−26 to −20	−10 to −1	−0.2	−1.9	−1.0
O	23.2759	120.2577	−13.8	6653 ± 56	7024–7285	−10 to −8	−3 to 0	−0.1	−0.8	−0.5
O1	23.2759	120.2577	−46.3	9284 ± 140	9532–10306		Using for correlation in Fig. 7			
P	23.2734	120.3125	−13.0	7201 ± 66	7869–8168	−16 to −14	−3 to 0	0.7	0.1	0.4
P-1	23.2734	120.3125	−29.6	9129 ± 58	9258–10267		Using for correlation in Fig. 7			
P-2	23.2734	120.3125	−62.0	43207 ± 1122			Using for correlation in Fig. 7			
P-3	23.2734	120.3125	−98.9	>50000			Using for correlation in Fig. 7			
Q	23.2865	120.3654	−4.3	7277 ± 66	7957–8189	−16 to −14	0–3	1.4	0.8	1.1
Q-1	23.2865	120.3654	−21.7	9345 ± 58	10292–10731		Using for correlation in Fig. 7			
R	23.2407	120.1256	−68.0	9030 ± 57	9137–9924	−30 to −23	−3 to 0	−3.5	−4.9	−4.2
S	23.2051	120.2064	−65.8	9660 ± 60	10111–11115	−49 to −32	−10 to −1	−0.6	−3.2	−1.9
T	23.2307	120.2610	−26.6	7415 ± 162	7874–8539	−18 to −14	−3 to 0	−0.7	−1.6	−1.1
U	23.2245	120.3505	6.3	7770 ± 40	8145–8330	−17 to −15	0–3	2.8	2.2	2.5
V	23.1829	120.1104	−59.2	8367 ± 60	8749–9267	−24 to −20	−10 to −1	−2.7	−4.4	−3.5
W	23.1871	120.2693	−18.0	6862 ± 99	7205–7555	−11 to −9	−3 to 0	−0.5	−1.2	−0.9
X	23.1494	120.1544	−83.9	10347 ± 82	10844–11906	−54 to −45	−10 to −1	−1.7	−3.5	−2.6
Y	23.1359	120.2874	−9.5	6204 ± 63	6909–7264	−9 to −7	−3 to 0	0.3	−0.4	0.0
Z	23.1388	120.3241	−4.7	8050 ± 40	8779–9028	−22 to −20	−3 to 0	2.2	1.7	2.0
AA	23.1052	120.0723	−59.1	8253 ± 67	8565–8940	−22 to −19	−10 to −1	−3.0	−4.6	−3.8
AB	23.1021	120.1178	−115.3	11957 ± 63	13047–13806	−73 to −63	−3 to 0	−2.8	−4.0	−3.4
AC	23.1234	120.1992	−75.8	9681 ± 63	10198–11119	−49 to −34	−10 to −1	−1.5	−4.0	−2.8
AD	23.0812	120.2180	−70.3	9375 ± 59	9711–10541	−40 to −28	−3 to 0	−2.6	−4.4	−3.5
AE	23.0425	120.0675	−88.9	9661 ± 71	10106–11117	−49 to −32	−3 to 0	−3.3	−5.6	−4.5

AF	23.0302	120.1351	−126.6	11190 ± 80	12359–13736	−72 to −58	−3 to 0	−3.8	−5.6	−4.7
AG	23.0395	120.1920	−74.4	8970 ± 60	9104–9841	−29 to −23	−10 to −1	−3.6	−5.6	−4.6
AH	22.9599	120.2218	−2.7	8320 ± 60	8647–9263	−24 to −19	−3 to 0	2.6	1.9	2.3

Location of sample site is shown in Fig. 6. All the data are reference from report of Central Geological Survey (Wu, 1999). The data also can be found in website (http://www.moeacgs.gov.tw).

[a] The sample elevation is calculated in relation to the modern sea level.

[b] Calibration curve of Stuiver and Reimer (1993).

[c] The reference of paleo-sea level curve is adopted from Chen and Liu (1996, 2000) and Hanebuth et al. (2000), as shown in Fig. 7.

[d] The depositional depth is assumed as 0–3 m for marsh, −3 to 0 m for estuary, lagoon and tidal-channel, −10 to −1 m for shoreface.

boreholes are plotted in Fig. 7 and located on the S–S′ profile. The lowstand erosion surface around 20 kyr and subsequent marine transgression can be clearly identified from the analysis of depositional environments and radiocarbon ages of the PL and TT domains. The 8 and 10 ka, horizons are shallower in the TT domain (wells P, Q) than in the PL domain (wells J, O), which agrees with the geomorphic characteristics presented above.

The results reveal that the TT domain is uplifting at a rate of 0.4–3.3 mm/yr. The PL domain is mainly subsiding with a rate of −0.2 mm/yr in its eastern part and gradually increasing up to −4.7 mm/yr westwards (Fig. 6). These values agree with the long-term (~20 kyr) vertical movement rates for the entire Coastal Plain of Taiwan calculated by Lai and Hsieh (2003). Subsidence can be related to formation of a foreland basin by loading of the thrust belt (Watts, 1992).

4. Discussion

4.1. The present deformation front

The drainage network is sensitive enough to reflect the regional variation of surface slopes. At an incipient stage the valley slope increases in response to tectonic uplift followed by an increase of the river sinuosity to maintain a constant gradient (Schumm and Khan, 1972; Burnett and Schumm, 1983; Ouchi, 1985). If the meander is under uniform uplift, the main channel cuts down to the level of the original surface, and consequently forms an incised meander. The newly developed tributaries also evolve into a dendritic pattern. As suggested by Phillips and Schumm (1987), the drainage pattern may change with the slope gradient: dendritic at 1%, sub-dendritic at 2%, sub-parallel at 3%, and parallel at 5% or higher slope.

In the TT domain, the regional slope has been tilted in a range of 0.1–1% producing an increase of the sinuosity of the main channel, development of erosional scarps in lateral sides of the channel, forming an incised meander on the tableland (Fig. 4b). Geomorphic processes such as river incision and patterns of calculated uplift, suggest that a NNE-trending active structure is present beneath the western part of the TT domain. This is consistent with other independent studies that are discussed below.

Geodetic measurements have been used to calculate movements in the study area (e.g. Yu and Chen, 1994; Yu et al., 1997; Hung et al., 1999; Hou et al., 2002). These studies indicate that the average horizontal velocity decreases from the LH domain (11–21 mm/yr), through the TT domain (5–9 mm/yr) to the PL domain (1–5 mm/yr) (Fig. 1). Crustal strain is mainly accommodated within the LH domain and TT domains, indicating that recent tectonic activity is located at the boundary faults (i.e. the Chiuchiungkeng fault and the Muchiliao–Liouchia faults in Fig. 3). At the boundary between the TT

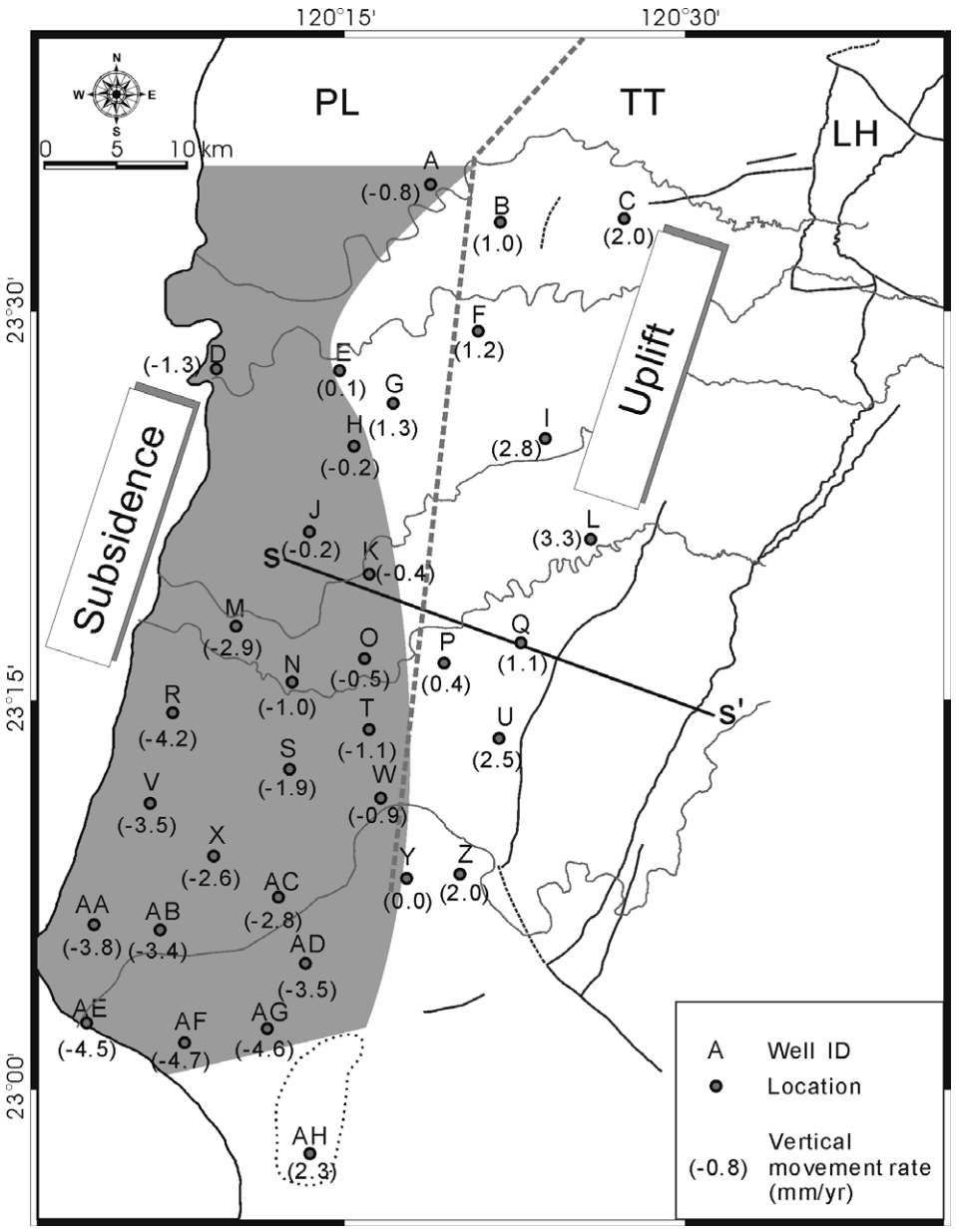

Fig. 6. Locations of 34 wells that are used to analyze vertical movement in each domain. Borehole data suggests that the TT domain is undergoing uplift, while PL domain, subsidence (shaded area). Active faults and rivers are shown in Figs. 2 and 4.

domain and PL domain, the shortening gradually decreases westwards.

Geomorphic studies of Holocene terraces exposed in the LH domain reveal very high uplift rates (5–7 mm/yr) (Chen, 1993; Liu et al., 1997; Hsieh and Knuepfer, 2002). These results, together with the rates of vertical crustal movement derived from the wells in this study, mark the shift from uplift to subsidence at the western margin of the TT domain. Since both uplift and shortening decrease strongly at the western margin of the TT domain, we infer the presence of a blind thrust at this location. Seismic exploration in the northern part of the study area identified a thrust fault, termed the Hsiaomei fault, beneath the front of the lateritic tableland (Hung et al., 1999). As a consequence, the TT domain and the LH domains are both situated in the hanging wall of this blind thrust and have undergone both horizontal shortening and uplift. The PL domain is situated in the footwall of the fault, and thus its location is consistent with subsidence recorded in this region. We suggest that the blind thrust defined in this study by geomorphology represents the active deformation front of the Taiwan orogen.

4.2. Segmented blind thrust system

The above-mentioned deformation front of Taiwan fold-and-thrust belt is located west of the present-day mountain front and probably delineated by a blind thrust beneath the

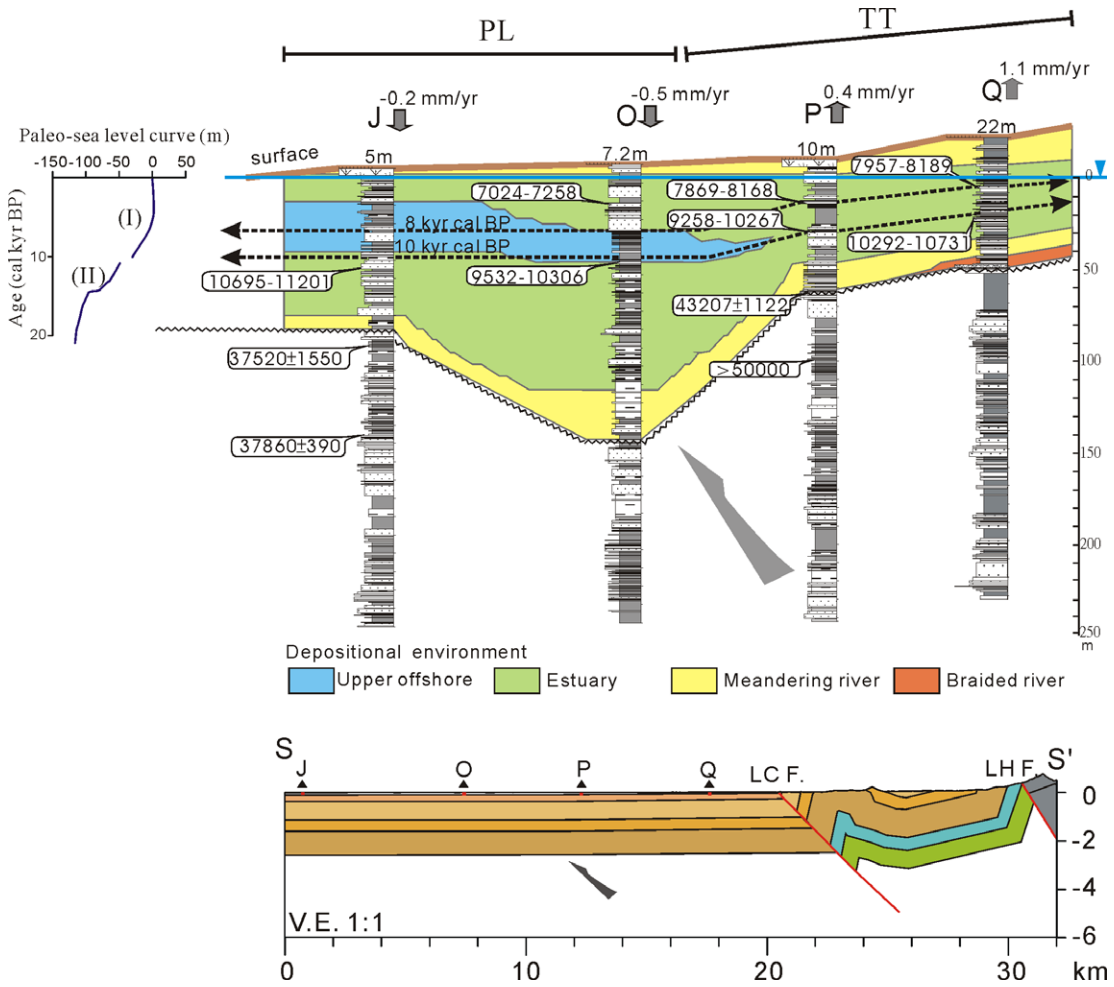

Fig. 7. Data of four boreholes projected onto S–S′ cross section (see in Fig. 6) are used to analyze vertical movement rates in PL and TT domains. The elevations of two synchronous horizons of marine sediments, aged 8 and 10 ka, respectively, are higher in the TT domain (P, Q; uplifting) than in the PL domain (J, O; subsidence), suggesting that a blind thrust may exist at the boundary between the two domains. Lowstand erosional surface is shown as a toothed line. The paleo-sea level curve (I) is adopted from Chen and Liu (1996, 2000), and (II) from Hanebuth et al. (2000).

Coastal Plain. However, the front does not display a continuous trace from north to south (Fig. 6). Our stratigraphic data indicate that the N–N′ and S–S′ cross sections illustrate different structure patterns (Fig. 3). The lateritic soils are only distributed in the north part of Chiayi block (Fig. 2). Geological evidence implies a longer period of crustal deformation in the northern part of the Chiayi block than in the southern one. There is an indentation of the uplifting area at 23°30′ latitude, that we interpret as segment boundary of the main thrust perhaps marking a strike-slip fault (Fig. 8). According to subsurface structural analysis, some strike-slip faults have been identified in the Coastal Plain (Biq, 1992; Lu, 1994; Lin and Huang, 1998).

Regional geology studies show that the Kukeng fault and the Hsinhua fault to the north and the south, respectively, are two major strike-slip faults bounding the block (Hung et al., 1999) (Fig. 8). The Meishan fault, which ruptured in the 1906 earthquake, is another major strike-slip fault within the study area. Many pre-existing E–W trending normal faults have been documented in southwestern Taiwan (Hsiao, 1971, 1974; Chow et al., 1988). Some of these may currently be reactivated as strike-slip structures. For instance, the Yichu fault may be a reactivated fault that contributes to the irregular shape of the deformation front.

5. Conclusions

Analysis of borehole data and stream drainage patterns suggests that southwestern part of the Coastal Plain is part of the Taiwan orogenic belt. We present evidence for a change from uplift in the LH and TT domains to subsidence in the PL domain that we interpret as caused by a blind thrust. This NNE–SSW trending thrust beneath the TT domain represents the deformation front of the Taiwan fold-and-thrust belt. The deformation front is thus located between the plain area and tilted tableland area of western Taiwan, westwards of where it had previously been defined. The frontal thrust may

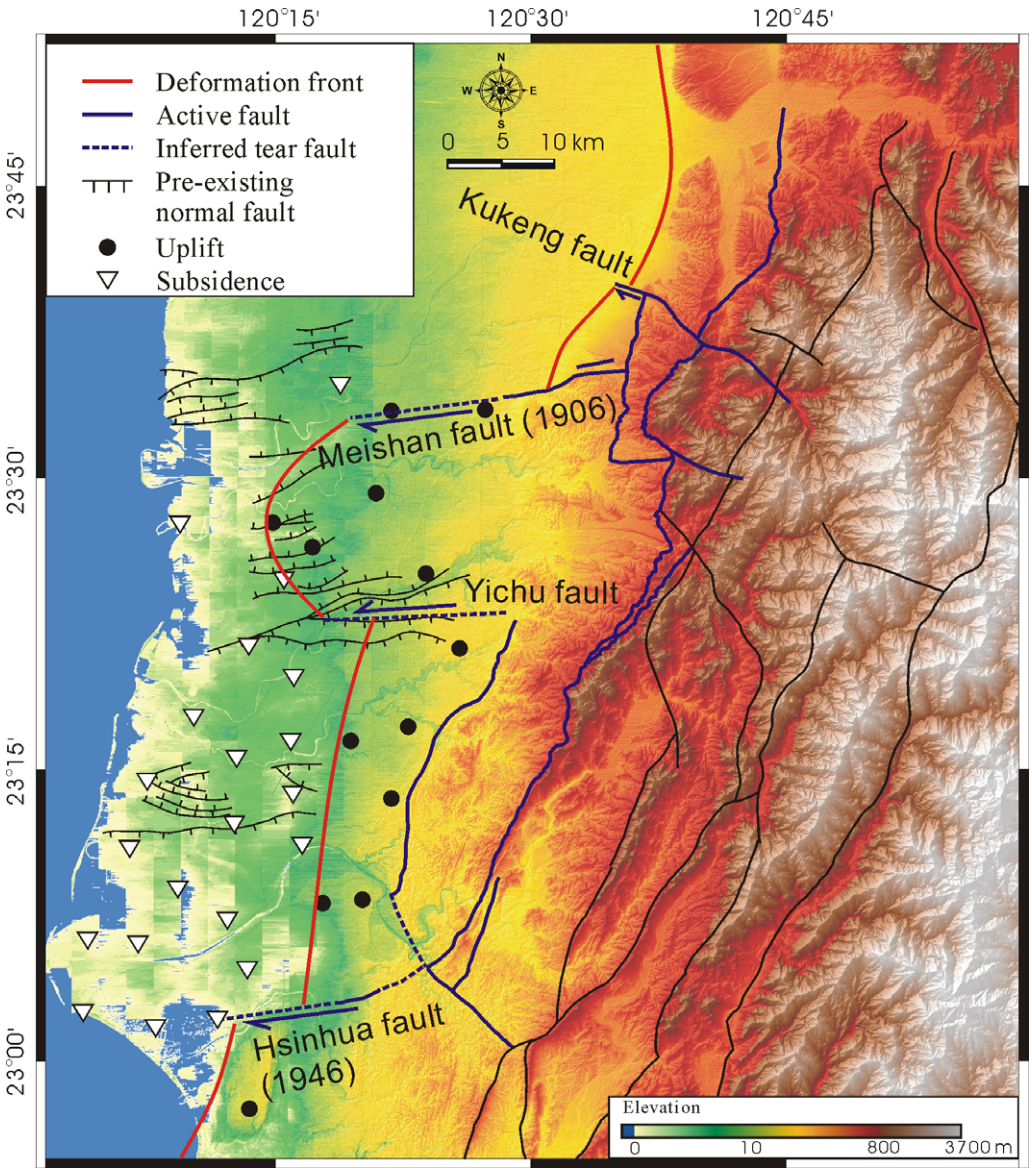

Fig. 8. Four major faults (Kukeng, Meishan, Yichu and Hsinhua faults) beneath the Chianan plain based on anomalously sharp contacts of strata are possibly pre-existing E–W striking high angle normal faults that are currently reactivated as strike-slip faults. These faults may segment the blind thrust that represents the fold-and-thrust front.

be segmented by, respectively, of E–W strike-slip faults. For example, the Kukeng fault and the Hsinhua faults bound the Chaiyi block to the north and the south, delineating a segment of the fold-and-thrust belt in southwestern Taiwan.

Acknowledgments

We thank Prof. Y. Ota, K. Berryman, and an anonymous reviewer for their critical reviews and helpful suggestions. Thanks also go to Prof. K. Mueller, and Y.-G. Chen for their editorial efforts. We are grateful to the assistants who participated in the field work. We also thank the Central Geological Survey of Taiwan for providing the well data. This research was supported by the National Science Council of Taiwan under Grant NSC-92-2116-M-002-001 and by Central Geological Survey of Taiwan Grant under CGS-91ECA38104.

References

Biq, C., 1991. Wrench-fault characteristics of the Meishan earthquake fault near Chia-I, Taiwan (in Chinese with English abstract). Ti-Chih 11, 111–119.

Biq, C., 1992. Another coastal range on Taiwan (in Chinese with English abstract). Ti-Chih 12, 1–14.

Bonilla, M.G., 1975. A review of recently active faults in Taiwan. United States Geological Survey Open-File Report 75–41, 1–72.

Burbank, D.W., Anderson, R.S., 2001. Tectonic Geomorphology. Blackwell Science, Massachusetts.

Burnett, A.W., Schumm, S.A., 1983. Alluvial river response to neotectonic deformation in Louisiana and Mississippi. Science 222, 49–50.

Chang, L.S., Chow, M., Chen, P.Y., 1947. The Tainan earthquake of December 5, 1946 (in Chinese with English abstract). Bulletin of the Central Geological Survey 1, 11–20.

Chen, Y.G., 1993. Sea-level change and neotectonics in southern part of Taiwan region since late Pleistocene (in Chinese). PhD thesis. Department of Geosciences, National Taiwan University, Taipei, Taiwan.

Chen, Y.G., Liu, T.K., 1996. Sea level changes in the last several thousand years, Penghu Islands, Taiwan Strait. Quaternary Research 45, 254–262.

Chen, Y.G., Liu, T.K., 2000. Holocene uplift and subsidence along an active tectonic margin southwestern Taiwan. Quaternary Science Reviews 19, 923–930.

Chen, Z.H., Chen, W.S., Wang, Y., Chen, M.M., 1992. Petrographical study of foreland sandstones and its relation to unroofing history of the fold-thrust belt in central Taiwan (in Chinese with English abstract). Ti-Chih 12, 147–165.

Chen, W.S., Erh, C.H., Chen, M.M., Yang, C.C., Chang, I.S., Liu, T.K., Horng, C.S., Shea, K.S., Yeh, M.G., Wu, J.C., Ko, C.T., Lin, C.C., Huang, N.W., 2000. The evolution of foreland basins in the western Taiwan: evidence from the Plio-Pleistoence sequences (in Chinese). Bulletin of the Central Geological Survey 13, 137–156.

Chen, W.S., Ridgway, K.D., Horng, C.S., Chen, Y.G., Shea, K.S., Yeh, M.G., 2001. Stratigraphic architecture, magnetostratigraphy, and incised-valley systems of the Pliocene-Pleistocene collisional marine foreland basin of Taiwan: Eustatic and tectonic controls on deposition. Geological Society of America Bulletin 113, 1249–1271.

Cheng, S.N., Yeh, Y.T., 1989. Catalog of the earthquakes in Taiwan from 1604 to 1988 (in Chinese). Institute of Earth Sciences, Academia Sinica, Taipei, pp. 1–255.

Chinese Petroleum Corporation, 1986. Geologic map of western Taiwan, Chiayi sheet (1:100,000). Taiwan Petroleum Exploration Division, Miaoli, Taiwan.

Chinese Petroleum Corporation, 1989. Geologic map of western Taiwan, Tainan sheet (1:100,000). Taiwan Petroleum Exploration Division, Miaoli, Taiwan.

Chow, J., Yang, K.M., Chen, H.M., 1988. Seismic interpretation of the subsurface structures in the Yichu-Chiali area, southern Taiwan. Petroleum Geology of Taiwan 24, 60–95.

Deffontaines, B., Lacombe, O., Angelier, J., Chu, H.T., Mouthereau, F., Lee, C.T., Deramond, J., Lee, J.F., Yu, M.S., Liew, P.M., 1997. Quaternary transfer faulting in the Taiwan Foothills: evidence from a multisource approach. Tectonophysics 274, 61–82.

Hanebuth, T., Statteffer, K., Grootes, P., 2000. Rapid flooding of the Sunda Shelf; a late-glacial sea-level record. Science 288, 1033–1035.

Ho, C.S., 1967. Structural evolution and major tectonic forms of Taiwan. Proceedings of the Geological Society of China 10, 3–24.

Hou, J.S., Wang, C.S., Fei, L.Y., 2002. Crustal deformation monitor by using GPS, southwestern Taiwan (in Chinese). 21th Applying Surveying conference, pp. 687–694.

Hsiao, P.T., 1971. Seismic study of the area between the coastal plain and the foothills, Yunlin, Taiwan. Petroleum Geology of Taiwan 8, 249–263.

Hsiao, P.T., 1974. Subsurface geologic study of the Hsinying coastal plain area, Taiwan. Petroleum Geology of Taiwan 11, 27–39.

Hsieh, M.L., Knuepfer, P.L.K., 2002. Synchronicity and morphology of Holocene river terraces in the southern Western Foothills, Taiwan: A guide to interpreting and correlating erosional river terraces across growing anticlines. In: Byrne, T.B., Liu, C.-S. (Eds.), Geology and Geophysics of an Arc-Continent Collision, Taiwan, vol. 358. Geological Society of America Special Paper, pp. 55–74.

Hsu, Y.J., Mark, S., Yu, S.B., Kuo, K.C., Chen, H.Y., 2003. A two-dimensional dislocation model for interseismic deformation of the Taiwan mountain belt. Earth and Planetary Science Letters 211, 287–294.

Hung, J.H., Wiltschko, D.V., Lin, H.C., Hickman, J.B., Fang, P., Bock, Y., 1999. Structure and motion of the southwestern Taiwan fold and thrust belt. Terrestrial, Atmospheric and Oceanic Sciences 10, 543–568.

Lai, T.H., Hsieh, M.L., 2003. Late-Quaternary vertical rock-movement rates of the coastal plains of Taiwan. 2003 Annual Meeting of the Geological Society of China, pp. 550–557.

Lin, C.W., Huang, M.L., 1998. Influence of the Peikang basement high on the structural development of Western Foothills and Coastal Plain in South Central Taiwan: a sandbox approach. Petroleum Geology of Taiwan 32, 105–122.

Lin, C.W., Chang, H.C., Lu, S.T., Shih, T.S., Huang, W.J., 2000. An Introduction to the Active Faults of Taiwan, 2nd ed. Special Publication of Central Geological Survey, 13, pp. 1–122.

Liu, T.K., Sung, Q.C., Chen, K.Y., Pi, Q.L., Yang, C.H., Chen, P.H., 1997. Tectonic subsidence and uplift in the Zeikang-Hopi area of southwestern Taiwan since the late Pleistocene. Journal of the Geological Society of China 40, 155–165.

Liu, C.S., Liu, S.Y., Lallemand, S.E., Lundberg, N., Reed, D., 1998. Digital elevation model offshore Taiwan and its tectonic implications. Terrestrial, Atmospheric and Oceanic Sciences 9, 705–738.

Lu, C.Y., 1994. Neotectonics in the foreland thrust belt of Taiwan. Petroleum Geology of Taiwan 29, 1–26.

Mouthereau, F., Deffontaines, B., Lacombe, O., Angelier, J., 2002. Variations along the strike of the Taiwan thrust belt: Basement control on structural style, wedge geometry, and kinematics. In: Byrne, T.B., Liu, C.-S. (Eds.), Geology and Geophysics of an Arc-Continent Collision, Taiwan, vol. 358. Geological Society of America Special Paper, pp. 31–54.

Ouchi, S., 1985. Response of alluvial rivers to slow active tectonic movement. Geological Society of America Bulletin 96, 504–515.

Phillips, L., Schumm, S.A., 1987. Effect of regional slope on drainage networks. Geology 15, 813–816.

Schumm, S.A., Khan, H.R., 1972. Experimental study of channel patterns. Geological Society of America Bulletin 83, 1755–1770.

Schumm, S.A., Dumont, J.E., Holbrook, J.M., 2000. Active Tectonics and Alluvial Rivers. Cambridge University Press.

Shirai, M., Tada, R., 2000. Sedimentary successions formed by fifth-order glacio-eustatic cycles in the middle to upper Quaternary formations of the Oga Peninsula, northeast Japan. Journal of Sedimentary Research 70, 839–849.

Shyu, J.B.H., Sieh, K., Chen, Y.G., Liu, C.S., 2005. Neotectonic architecture of Taiwan and its implications for future large earthquakes. Journal of Geophysical Research-Solid Earth 110, B08402.

Stuiver, M., Reimer, P.J., 1993. Extended ^{14}C data base and revised CALIB 3.0 ^{14}C age calibration program. Radiocarbon 35, 215–230.

Sun, S.C., 1970. Photogeologic study of the Tainan–Hsinying coastal plain area, Taiwan. Petroleum Geology of Taiwan 7, 133–144.

Sun, S.C., 1971. Photogeologic study of the Hsinying–Chiayi coastal plain area, Taiwan. Petroleum Geology of Taiwan 8, 65–75.

Sun, R., Sung, Q.C., Liu, T.K., 1998. Near-surface evidence of recent Taiwan Orogeny detected by a shallow seismic method. Earth and Planetary Science Letters 163, 291–300.

Suppe, J., 1981. Mechanics of mountain building and metamorphism in Taiwan. Memoir of the Geological Society of China 4, 67–89.

Suppe, J., 1984. Kinematics of arc-continent collision, flipping of subduction, and back arc spreading near Taiwan. Memoir of the Geological Society of China 6, 21–24.

Teng, L.S., 1990. Geotectonic evolution of late Cenozoic arc-continental collision in Taiwan. Tectonophysics 183, 67–76.

Teng, L.S., Lee, C.T., Tsai, Y.B., Hsiao, L.Y., 2000. Slab breakoff as a mechanism for flipping of subduction polarity in Taiwan. Geology 28, 155–158.

Watts, A.B., 1992. The effective elastic thickness of the lithosphere and the evolution of foreland basins. Basin Research 4, 169–178.

Wu, L.C., 1999. Sedimentary environment analysis and stratigraphic correlation in Chianan coastal plain (in Chinese). Central Geological Survey report 88–015, 1–212.

Yang, C.C.B., Yen, I.C., Chen, W.S., Lin, C.W., 2003. Chiuchiungkeng Fault: Evidence from field investigation and paleoseismic trenching (in Chinese). 2003 Annual Meeting of the Geophysical Society of China, pp. 422–426.

Yeh, Y.H., Chen K.J., Wang, W.H., Tsai, Y.B., 1984. The Survey of the 1906 Meishan Earthquake Fault in Chiayi (in Chinese). Institute of Earth Sciences, Academia Sinica, Taipei, pp. 1–75.

Yu, S.B., Chen, H.Y., 1994. Global positioning system measurements of crustal deformation in the Taiwan arc-continent collision zone. Terrestrial, Atmospheric and Oceanic Sciences 5, 477–498.

Yu, S.B., Chen, H.Y., Kuo, L.C., 1997. Velocity of GPS stations in the Taiwan area. Tectonophysics 274, 41–59.